ACS APPLIED MATERIALS & INTERFACES

Research Article

www.acsami.org

Superior Properties of Energetically Stable $La_{2/3}Sr_{1/3}MnO_3$/Tetragonal $BiFeO_3$ Multiferroic Superlattices

Nan Feng,[†] Wenbo Mi,*[,†] Xiaocha Wang,[‡] Yingchun Cheng,[§,∥] and Udo Schwingenschlögl*[,∥]

[†]Tianjin Key Laboratory of Low Dimensional Materials Physics and Preparation Technology, Faculty of Science, Tianjin University, Tianjin 300072, China

[‡]Tianjin Key Laboratory of Film Electronic & Communicate Devices, School of Electronics Information Engineering, Tianjin University of Technology, Tianjin 300384, China

[§]Department of Mechanical and Industrial Engineering, University of Illinois at Chicago, Chicago, Illinois 60607, United States

[∥]PSE Division, KAUST, Thuwal 23955-6900, Kingdom of Saudi Arabia

ABSTRACT: The superlattice of energetically stable $La_{2/3}Sr_{1/3}MnO_3$ and tetragonal $BiFeO_3$ is investigated by means of density functional theory. The superlattice as a whole exhibits a half-metallic character, as is desired for spintronic devices. The interfacial electronic states and exchange coupling are analyzed in details. We demonstrate that the interfacial O atoms play a key role in controlling the coupling. The higher ferroelectricity of tetragonal $BiFeO_3$ and stronger response to the magnetic moments in the $La_{2/3}Sr_{1/3}MnO_3/BiFeO_3$ superlattice show a strongly enhanced electric control of the magnetism as compared to the rhombohedral one. Therefore, it is particularly practical interest in the magnetoelectrically controlled spintronic devices.

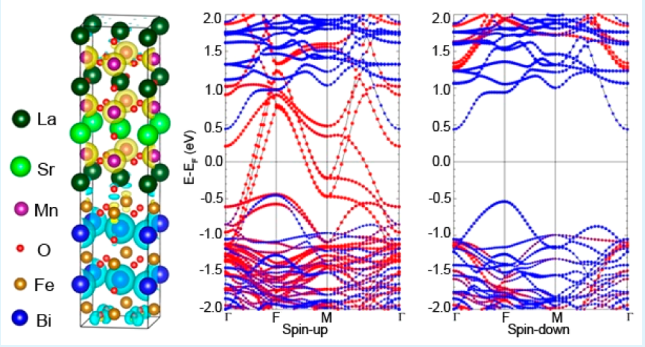

KEYWORDS: *multiferroic, electronic structure, magnetic properties, spintronics, interfacial coupling*

INTRODUCTION

Multiferroic materials display several long-range orders, such as ferromagnetism, ferroelectricity, and ferroelasticity. Combination of the ferromagnetic and ferroelectric couplings allows the magnetization to be tuned by an electric field and vice versa.[1−3] Such electric control of the magnetism has the potential applications in data storage as well as high-frequency magnetic devices with small currents and fields for operation.[4] The perovskite $La_{2/3}Sr_{1/3}MnO_3$ (LSMO) is a promising candidate in spintronic devices, because of its 100% spin polarization of the charge carriers and high ferromagnetic Curie temperature of T_C = 370 K.[5] The charge-mediated magnetoelectric effect has been demonstrated in the epitaxial $LSMO/Pb(Zr_{0.52}Ti_{0.48})O_3$.[6,7] The observed magnetoelectric coupling in the $LSMO/BaTiO_3$ heterostructures has been attributed to the interfacial strains.[8] $BiFeO_3$ (BFO) is the only known single-phase multiferroic material with a high ferroelectric T_C = 1103 K and high G-type antiferromagnetic Néel temperature of 643 K.[9,10] Unfortunately, it suffers from weak magnetoelectric response and low electrical resistivity.[11,12] An alternative pathway to realize the magnetoelectric control is the exchange bias when a ferromagnetic material is coupled with the antiferromagnetic BFO.[13,14] Electric control exchange bias has been demonstrated for a heterostructure of LSMO and rhombohedral BFO, which may lead to low power devices with smaller size.[15,16] Additionally, Béa et al. have reported that the LSMO/BFO bilayers have a high and homogeneous resistivity state of the BFO as a ferroelectric tunnel barrier.[17] Jilili et al. have found that the LSMO/rhombohedral BFO superlattice maintains the half-metallic character of bulk LSMO.[18] Moreover, Guo et al. have discovered that the anomalies in the temperature-dependent ferromagnetic resonance spectra of LSMO occur at the transition temperature of Fe polarization, indicating a strong interfacial coupling between Fe and Mn.[19] Yu et al. have reported a significant exchange bias for the coupling between LSMO and rhombohedral BFO using the X-ray circular dichroism method.[20] Concerning the origin of the interfacial Fe magnetic ordering, several physical mechanisms have been proposed, including the strong Mn−Fe hybridization,[20] Fe−O−Fe bond angle alteration and suppression of octahedral tiltings close to the interface,[21] charge and orbital ordering,[11] and Fe/Mn intermixing.[22]

It is found that the spontaneous polarization of tetragonal BFO is 150 $\mu C/cm^2$, which is much higher than the value of the rhombohedral structure (90 $\mu C/cm^2$).[23,24] Zhang et al. have experimentally evidenced that the ferroelectric polarization of tetragonal BFO grown on $LaAlO_3$ substrate is significantly enhanced and have attributed it to pronounced the strain-

Received: March 19, 2015
Accepted: April 30, 2015
Published: April 30, 2015

DOI: 10.1021/acsami.5b02436
ACS Appl. Mater. Interfaces 2015, 7, 10612−10616

induced Fe displacements relative to the O octahedron.[25] Sun et al. have reported a significantly enhanced exchange bias in bilayers of Fe_3O_4 and tetragonal BFO and have attributed to stronger Fe−O−Fe interfacial superexchange in the distorted structure.[26] If highly spin-polarized LSMO is deposited on tetragonal BFO epitaxially, a strongly enhanced electric control of the magnetism may be realized, which has great potential applications in the spintronic devices. Thus, in this work, we study the interfacial electronic and magnetic properties of the LSMO/tetragonal BFO superlattices by density functional theory, demonstrating a remarkable magnetoelectric effect.

CALCULATION DETAILS AND MODELS

We perform the density functional theory[27] calculations using the projector augmented wave method[28] and Perdew−Burke−Ernzerhof[30] spin-polarized generalized gradient approximation (GGA) as implemented in the Vienna Ab initio Simulation Package.[29] To account for the localized *d* orbitals of the transition metals, we consider an on-site Coulomb interaction *U*. We set U = 2 eV for Mn and U = 4.5 eV for Fe, based on the previous theoretical studies for bulk LSMO and BFO.[13,14,31] We have confirmed that the adopted GGA functional can give a reliable description of the half-metallicity of LSMO[32] as well as antiferromagnetic ordering, ferroelectricity and band gap of BFO. We employ the valence electron configurations O $2s^2 2p^4$, Mn $3d^6 4s^1$, Fe $3d^7 4s^1$, Sr $4s^2 4p^6 5s^2$, La $5p^6 5d^1$, and Bi $6s^2 6p^3$. The calculations are performed with a plane wave cutoff energy of 500 eV, where Γ-centered 9 × 9 × 9 and 9 × 9 × 1 *k*-meshes are used for the bulk compounds and the superlattice, respectively. The convergence criterion for the energy is set to 1×10^{-5} eV and that for the atomic forces to 0.01 eV/Å.

Tetragonal BFO with space group *P4mm* has lattice constants of a = 3.94 Å and c/a = 1.02,[33,34] where the O_A and O_B, respectively, belong to the BiO and FeO layers, see Figure 1a. It is not clear which antiferromagnetic order of G-type or C-type film in the tetragonal phase would show.[35] In this work, we consider G-type antiferromagnetism, in which the magnetic moments of Fe atoms align ferromagnetically in (111) planes and antiferromagnetically between adjacent (111) planes.[36] Bulk LSMO has a tetragonal structure (space group *P4mm*) with the lattice constants a = 3.88 Å and c/a = 3.00.[37] The unit cell contains four layers: SrO, LaO, Mn_AO_2 and Mn_BO_2, see Figure 1b. The Mn_A atom sees a SrO layer below and a LaO layer on top, whereas the Mn_B atom sees LaO layers on both sides. We model the superlattice using a slab geometry with seven LSMO and five BFO layers, based on a $\sqrt{2} \times \sqrt{2}$ in-plane supercell for accommodating the BFO's G-type antiferromagnetic ordering. The surface unit cell of BFO(001) has $\sqrt{2} \times \sqrt{2}R45°$ periodicity with lattice constant 5.57 Å, whereas the surface unit cell of LSMO(001) has the same periodicity with a lattice constant of 5.49 Å, i.e., the lattice mismatch is less than 1.5%. This allows us to use the average lattice constant for the *ab*-plane.

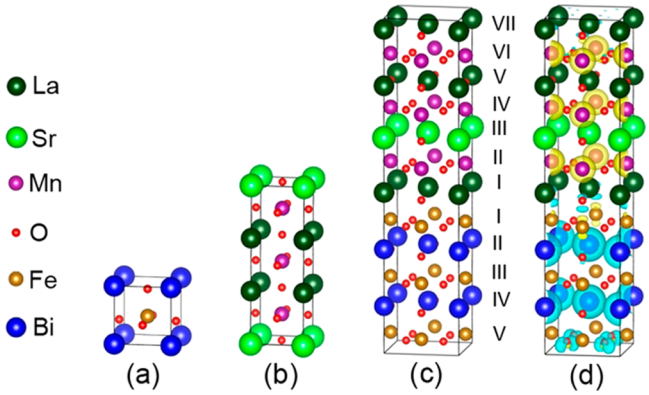

Figure 1. Structures of (a) bulk BFO, (b) bulk LSMO, and (c) the LSMO/BFO superlattice. (d) Charge density difference (isosurface value 0.01 e/Å^3) for the LSMO/BFO superlattice relative to the two components. Yellow regions represent the charge accumulation and blue regions charge depletion.

Eight stacking patterns with different terminations of LSMO on BFO can be realized: LSMO(001) with SrO, LaO, Mn_AO_2, and Mn_BO_2 terminations and BFO(001) with BiO_A and $Fe(O_B)_2$ terminations. As periodic boundary conditions are applied in all the directions, two interfaces are present in each supercell, which are inequivalent in an asymmetric structure.

RESULTS AND DISCUSSION

The most stable structure is determined by calculating the work of separation, i.e., the cohesive energy between LSMO and BFO, $W_{sep} = (E_{LSMO/BFO} - E_{LSMO} - E_{BFO})/2$, where $E_{LSMO/BFO}$ is the total energy of the superlattice and E_{LSMO} and E_{BFO} are the energies of the same supercell containing only relaxed LSMO and BFO, respectively.

The factor 1/2 accounts for the two interfaces per supercell. The energetically favorable configuration after the structural optimization, see Figure 1c, is LaO-terminated with interfacial O atoms located on top of interfacial Fe atoms and has W_{sep} = −5.13 eV. This is consistent with previous findings for a supercell consisting of LSMO and rhombohedral BFO[18,22] and a similar LSMO/$YMnO_3$ system,[38] in which the LaO-terminated interface has always the lowest energy. The largest work of separation suggests that this configuration is the most stable structure that occurs during the growth. The average interplanar spacing of the LaO and FeO_2 layers (both labeled I in Figure 1c) is 1.93 Å and that of the LaO and FeO_2 layers (labeled VII and V in Figure 1c) is 1.56 Å. More specifically, the O atoms are shifted out of the cationic plane, see Table 1. For BFO region, the relative Fe−O and Bi−O displacements are much smaller than the ferroelectric displacement in bulk BFO along [001] direction (0.61 and 0.79 Å, respectively). Therefore, the BFO is subjected to a reduced ferroelectric polarization. Furthermore, the O atoms in BFO region are displaced away from layer I, indicating a net polarization in BFO pointing to layer V. For LSMO region, in layer I, they shift heavily by 0.49 Å toward Fe atoms, whereas layer VII stays almost planar. As a result, the Fe−O bond lengths through the two interfaces amount to 1.93 and 2.31 Å, respectively. The former is slightly shorter than bulk FeO (2.16 Å),[39] indicative of a relatively strong interaction between adjacent Fe and O atoms. The huge shifts of the O atoms can be expected to determine the interfacial properties, because these atoms mediate the interaction between LSMO and BFO.

Figure 2a, b shows the total and projected densities of states (DOS) of fully relaxed bulk BFO and LSMO, respectively. For BFO, the calculated band gap of 1.90 eV is in excellent agreement with previous calculations[13] but does not reach the experimental value of 2.50 eV,[40] because of the limitations of the exchange and correlation functional in reproducing the derivative discontinuity.[41] Bi s states has negligible contribution to the bonding. The Fe spins are directed antiparallel but the DOS is the same, so we show only one atom. The calculated Fe magnetic moment in bulk BFO is ±4.18 μ_B/atom, agreeing well with a previously reported value.[33] The LSMO DOS exhibits a half-metallic character with a spin-down band gap of 1.87 eV. The magnetic moments of 3.42 and 3.68 μ_B are obtained for Mn_A and Mn_B, respectively. These values are close to the experimental value of 3.70 μ_B.[42] These results confirm the

DOI: 10.1021/acsami.5b02436
ACS Appl. Mater. Interfaces 2015, 7, 10612−10616

Table 1. Average Vertical Distances d_z and d_z' (in Å) of the O Plane Relative to Its Cationic Plane in the BFO and LSMO Regions of the Tetragonal LSMO/BFO Superlattice, see Figure 1c[a]

system		bulk	I	II	III	IV	V	VI	VII
tetragonal	d_z	−0.61/−0.79	−0.02	−0.45	−0.28	−0.43	−0.35		
	d_z'	0	+0.49	+0.28	+0.19	−0.07	+0.07	+0.14	0
	Mn	3.42/3.68		3.84				3.23	
	O	0.01	−0.11	−0.01				−0.02	0
rhombohedral	Mn	3.42/3.68		3.47				3.52	
	O	0.01	−0.07	−0.02				−0.01	0.05

[a]Positive/negative numbers denote shifts towards/off the Fe atoms in layer I. Comparison of the calculated magnetic moments (in μ_B) of Mn and O atoms near the interfaces in LSMO/BFO superlattice with tetragonal or rhombohedral BFO.

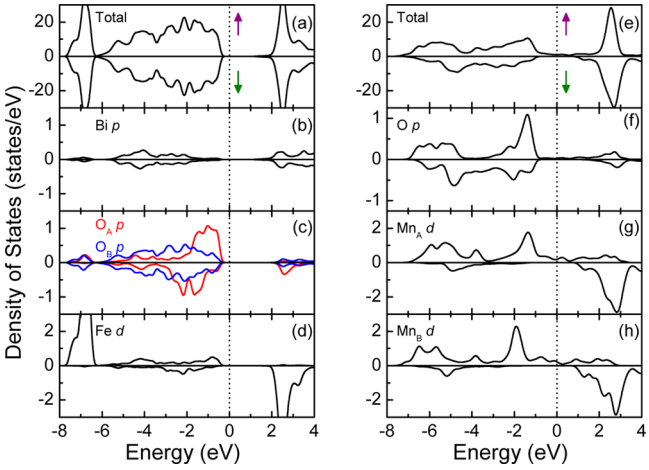

Figure 2. Total and partial PDOS of (a−d) bulk BFO and (e−h) bulk LSMO. The Fermi energy is indicated by vertical dashed lines and is set to zero.

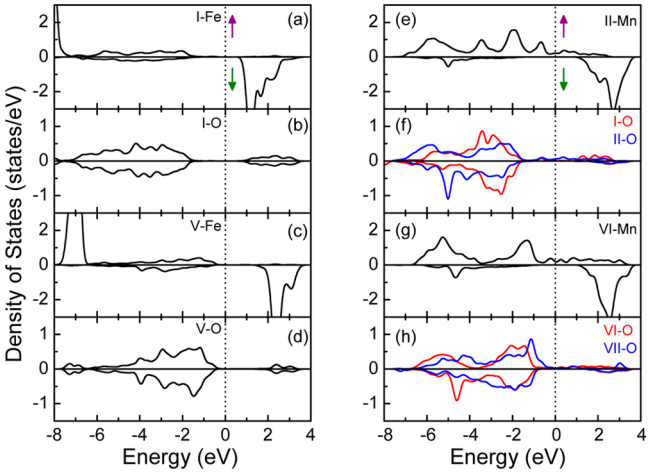

Figure 4. Partial DOS for the interfacial (a−d) BFO and (e−h) LSMO layers in the fully relaxed LSMO/BFO superlattice. The Fermi energy is indicated by vertical dashed lines and is set to zero.

rationality of the adopted parameters in the present calculations.

The band structure, partial DOS, and charge density difference obtained for the energetically favorable configuration of the superlattice are addressed in Figures 3, 4, and 1d, respectively. In Figure 3, the red and blue dots represent contributions of LSMO and BFO to the eigenstates, respectively, where the size quantifies the contribution. For

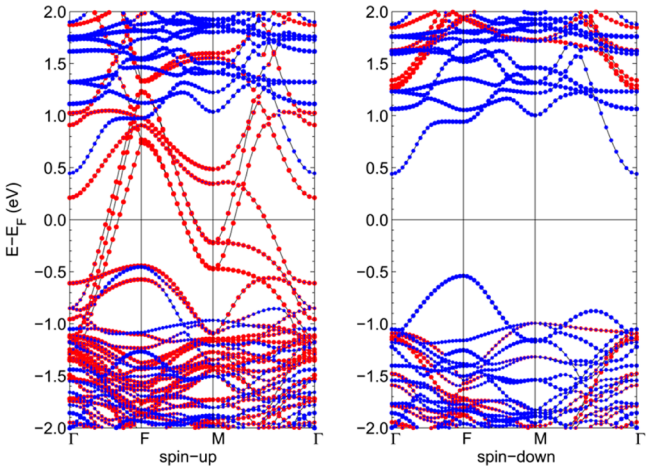

Figure 3. Spin-up and spin-down band structures of the LSMO/BFO superlattice. The size of the blue dots is proportional to the BFO contribution, whereas that of the red dots is proportional to the LSMO contribution.

BFO, the spin-up bands cross the Fermi level, exhibiting a metallic character, whereas the spin-down channel is semiconducting with a band gap of 0.98 eV, constituting a half-metallic character. LSMO is also half-metallic with a spin-down band gap of 2.3 eV. Thus, the entire superlattice is half-metallic, as is desired for the spintronic devices.

As compared to bulk LSMO, the magnetic moments in the superlattice decrease slightly. Because the bulk-like inner atomic layers nicely reproduce the bulk properties, we focus on the atoms close to the interface. In Figure 4, the lable I−Fe, for example, refers to the Fe atom in layer I, as defined in Figure 1c. Again, we address only one of the antiferromagnetically ordered Fe atoms. For BFO, Fermi level differs from the bulk: In layer I it shifts to higher energy by 1.16 eV, whereas in layer V, it is not shifted. The Fermi level upshift makes the orbital energies of the Fe d states in layer I close to O p states in layer I of LSMO, which enhances the energetic overlap between them. Hence, the Fe−O hybridization through the interface appears. Although there is no direct bonding between Mn in layer II and Fe in layer I, the indirect coupling mediated by O in layer I has a sizable effect on the Mn d states. The hybridization of Mn in layer II with O in layers I and II is slightly weaker than in the bulk, which enhances the magnetic moment to 3.84 μ_B and induces a huge O magnetic moment of 0.11 μ_B with opposite sign. We find strong hybridization between Mn in layer VI and O in layer VII in the whole energy range and between Mn in layer VI and O in layer V through the interface in valence band, as shown in Figure 4d, g, and h. This reduces the Mn magnetic moment to 3.23 μ_B. The hybridization between O and Fe in

DOI: 10.1021/acsami.5b02436
ACS Appl. Mater. Interfaces 2015, 7, 10612−10616

layers I and V does not change with respect to bulk so that the Fe magnetic moments retain their bulk values. The half-metallicity in BFO results from the contributions of the spin-up Fe d states in layer I and O p states in layer V because of the strong hybridization with O in layer I and Mn in layer VI. We note that as a result of the exchange coupling, the LSMO magnetization varies significantly near the two interfaces: Mn in layer II (VI) gains a magnetic moment of 0.42 (−0.45) μ_B, and the change of O magnetic moment is −0.12 μ_B for layer I and −0.03 μ_B for layer VI (see Table 1). This suggests that, when an electric field is applied to this configuration so as to reverse the ferroelectric polarization of BFO, the variation in the interfacial exchange coupling will modify the interfacial magnetization.

To judge the feasibility of the use of tetragonal BFO in the LSMO/BFO superlattice that can improve the magnetoelectric coupling, we have also analyzed the rhombohedral BFO for comparison. The rhombohedrally distorted perovskite BFO (space group: *R*3*c*) has the lattice constants of a = 3.96 Å and α = 89.5°.[43] For the rhombohedral superlattice, we use the same computational setup as that in the tetragonal LSMO/BFO superlattice. We find an asymmetry between Mn magnetic moments near two interfaces, 3.47 and 3.52 μ_B for layers II and VI, respectively, so that the change is 0.05 μ_B for layer II and −0.16 μ_B for layer VI with respect to bulk value. Jilili et al. have found that the difference in the Mn magnetic moments near two interfaces is 0.33 and 0.38 μ_B, respectively.[18] Neumann et al. have found that the change is about 0.15 μ_B.[22] Importantly, we note that the use of tetragonal BFO yields a stronger response to the variation of magnetic moment than the rhombohedral BFO, indicating a larger magnetoelectric effect. Our calculated work of separation for the interface between LSMO and rhombohedral BFO is −6.12 eV, which has the same sign as the interface to the tetragonal BFO, suggesting that both the interfaces are thermodynamically stable. The different phases of the BFO layer in the stack determine the ferroelectric polarization and subsequently the heterostructure's properties. A high-quality tetragonal BFO film has been grown on $LaAlO_3$ substrate by pulsed laser deposition[25] or magnetron sputtering,[26] so that one can deposit epitaxial LSMO layers on tetragonal BFO because of the good lattice match. Stronger magnetoelectric effect in the tetragonal BFO/LSMO heterostructures will stimulate further interest in developing the magnetoelectrically controlled spintronic devices. We believe that our theoretical prediction on the magnetoelectric effects provide useful information for experiments.

The detailed nature of the interaction at the LSMO/BFO interfaces is illustrated by the difference of the charge densities of the isolated LSMO and BFO slabs and that of the superlattice, see Figure 1d. We find a significant charge accumulation around Fe in layer I and around Mn in layer II, whereas O in layer I looses charge. The charge of O in layer V is redistributed to O in layer VII and to MnO_2 in layer VI. As discussed previously, the spontaneous polarization of BFO points toward layer V. Depositing LSMO atop BFO, the polar discontinuity at the interface results in the divergence of the electrostatic potential when the number of BFO layers grows because of the periodic boundary conditions. Electrons in BFO are transferred across the interface into LSMO region to form a build-in electric field pointing from BFO to LSMO for avoiding the divergence. Therefore, charge accumulates in deeper Mn layers and charge depletes in deeper Bi layers. The appearance of magnetoelectric effect in the heterostructures composed of LSMO and tetragonal BFO is consistent with the experimental findings in the similar LSMO/$Pb(Zr_{0.52}Ti_{0.48})O_3$ and LSMO/$BaTiO_3$ heterostructures.[6−8] The use of BFO in its tetragonal phase in LSMO/BFO heterostructures yields a more remarkable magnetoelectric effect than the rhombohedral BFO. Meanwhile, a significantly enhanced exchange bias in bilayers of Fe_3O_4 and tetragonal BFO compared to that of the rhombohedral BFO has also been observed experimentally.[26]

CONCLUSION

In conclusion, the density functional theory has been used to study the structural stability and electronic properties of the tetragonal LSMO/BFO(001) superlattice. The energetically favorable interface is found to consist of LaO-terminated LSMO and FeO_2-terminated BFO. The superlattice shows a half-metallicity and the interfacial exchange coupling (Fe−O−Mn) increases the Mn magnetic moment and induces a huge O magnetic moment of 0.11 μ_B. The surprising half-metallicity in the BFO domain originates from specific modifications of the orbital hybridizations because of the interaction with LSMO. It turns out that the interfacial O atoms and their spatial shifts play a key role in mediating the interaction and thus in the exchange mechanism. The tetragonal LSMO/BFO(001) superlattice is characterized by a strongly enhanced electric control of the magnetism and therefore is of particular practical interest in magnetoelectrically controlled spintronics.

AUTHOR INFORMATION

Corresponding Authors

*E-mail: miwenbo@tju.edu.cn.

*E-mail: Udo.Schwingenschlogl@kaust.edu.sa.

Author Contributions

N.F. and W.M. designed the outline of the manuscript and wrote the main manuscript text. X.W., Y.C., and U.S. contributed detailed discussions and revisions. All authors reviewed the manuscript.

Notes

The authors declare no competing financial interest.

ACKNOWLEDGMENTS

W. M. was supported by the NSFC of China (51171126), Key Project of TSTC of Tianjin (12JCZDJC27100 and 14JCZDJC37800), Program for NCET in University (NCET-13-0409), and Scientific Research Foundation for the Returned Overseas Chinese Scholars, State Education Ministry of China. It is also supported by High Performance Computing Center of Tianjin University, China. Research reported in this publication was supported by the King Abdullah University of Science and Technology (KAUST).

REFERENCES

(1) Eerenstein, W.; Mathur, N. D.; Scott, J. F. Multiferroic and Magnetoelectric Materials. *Nature* **2006**, *442*, 759−765.

(2) Fiebig, M. Revival of the Magnetoelectric Effect. *J. Phys. D* **2005**, *38*, R123−R152.

(3) Spaldin, N. A.; Fiebig, M. The Renaissance of Magnetoelectric Multiferroics. *Science* **2005**, *309*, 391−392.

(4) Huijben, M.; Yu, P.; Martin, L. W.; Molegraaf, H. J. A.; Chu, Y. H.; Holcomb, M. B.; Balke, N.; Rijnders, G.; Ramesh, R. Ultrathin Limit of Exchange Bias Coupling at Oxide Multiferroic/Ferromagnetic. *Adv. Mater.* **2013**, *25*, 4739−4745.

(5) Bowen, M.; Barthélémy, A.; Bibes, M.; Jacquet, E.; Contour, J. P.; Fert, A.; Ciccacci, F.; Duò, L.; Bertacco, R. Spin-Polarized Tunneling

DOI: 10.1021/acsami.5b02436
ACS Appl. Mater. Interfaces 2015, 7, 10612−10616

Spectroscopy in Tunnel Junctions with Half-Metallic Electrodes. *Phys. Rev. Lett.* **2005**, *95*, 137203.
(6) Mukherjee, D.; Hordagoda, M.; Lampen, P.; Phan, M. H.; Srikanth, H. Simultaneous enhancements of polarization and magnetization in epitaxial $Pb(Zr_{0.52}Ti_{0.48})O_3/La_{0.7}Sr_{0.3}MnO_3$ multiferroic heterostructures enabled by ultrathin $CoFe_2O_4$ sandwich layers. *Phys. Rev. Lett.* **2015**, *91*, 054419.
(7) Dussan, S.; Kumar, A.; Scott, J. F.; Katiyar, R. S. Magnetic effects on dielectric and polarization behavior of multiferroic heterostructures. *Appl. Phys. Lett.* **2010**, *96*, 072904.
(8) Eerenstein, W.; Wiora, M.; Prieto, J. L.; Scott, J. F.; Mathur, N. D. Giant sharp and persistent converse magnetoelectric effects in multiferroic epitaxial heterostructures. *Nat. Mater.* **2007**, *6*, 348−351.
(9) Choi, W. S.; Jeong, D. W.; Seo, S. S. A.; Lee, Y. S.; Kim, T. H.; Jang, S. Y.; Lee, H. N.; Myung-Whun, K. Charge States and Magnetic Ordering in $LaMnO_3/SrTiO_3$ Superlattices. *Phys. Rev. B* **2011**, *83*, 195113.
(10) Garcia-Barriocanal, J.; Cezar, J. C.; Bruno, F. Y.; Thakur, P.; Brookes, N. B.; Utfeld, C.; Rivera-Calzada, A.; Giblin, S. R.; Taylor, J. W.; Duffy, J. A.; Dugdale, S. B.; Nakamura, T.; Kodama, K.; Leon, C.; Okamoto, S.; Santamaria, J. Spin and Orbital Ti Magnetism at $LaMnO_3/SrTiO_3$ Interfaces. *Nat. Commun.* **2010**, *1*, 82.
(11) Calderón, M. J.; Liang, S.; Yu, R.; Salafranca, J.; Dong, S.; Yunoki, S.; Brey, L.; Moreo, A.; Dagotto, E. Magnetoelectric Coupling at the Interface of $BiFeO_3/La_{0.7}Sr_{0.3}MnO_3$ multilayers. *Phys. Rev. B* **2011**, *84*, 024422.
(12) Higuchi, T.; Liu, Y. S.; Yao, P.; Glans, P. A.; Guo, J.; Chang, C. L.; Wu, Z. Y.; Hattori, T. Electronic Structure of Multiferroic $BiFeO_3$ by Resonant Soft X-Ray Emission Spectroscopy. *Phys. Rev. B* **2008**, *78*, 085106.
(13) Yang, H.; Jin, C.; Mi, W. B.; Bai, H. L.; Chen, G. F. Electronic and Magnetic Structure of $Fe_3O_4/BiFeO_3$ Multiferroic Superlattices: First Principles Calculations. *J. Appl. Phys.* **2012**, *112*, 063925.
(14) Feng, N.; Mi, W. B.; Wang, X. C.; Bai, H.L. The Magnetism of Fe_4N/oxides (MgO, $BaTiO_3$, $BiFeO_3$) Interfaces from First-principles Calculations. *RSC Adv.* **2014**, *4*, 48848−48859.
(15) Wu, S. M.; Cybart, S. A.; Yu, P.; Rossell, M. D.; Zhang, J. X.; Ramesh, R.; Dynes, R. C. Reversible Electric Control of Exchange Bias in a Multiferroic Field-Effect Device. *Nat. Mater.* **2010**, *9*, 756−761.
(16) Wu, S. M.; Cybart, S. A.; Yi, D.; Parker, J. M.; Ramesh, R.; Dynes, R. C. Full Electric Control of Exchange Bias. *Phys. Rev. Lett.* **2013**, *110*, 067202.
(17) Béa, H.; Bibes, M.; Sirena, M.; Herranz, G.; Bouzehouane, K.; Jacquet, E.; Fusil, S.; Paruch, P.; Dawber, M.; Contour, J. P.; Barthélémy, A. Combining Half-Metals and Multiferroics into Epitaxial Heterostructures for Spintronics. *Appl. Phys. Lett.* **2006**, *88*, 062502.
(18) Jilili, J.; Eckern, U.; Schwingenschlögl, U. Half-Metallicity in a $BiFeO_3/La_{2/3}Sr_{1/3}MnO_3$ Superlattice: A First-Principles Study. *EPL* **2013**, *102*, 67009.
(19) Guo, H. Y.; Lin, J. G.; Yang, J. C.; Chu, Y. H. Dynamic Magnetic Interaction in $La_{2/3}Sr_{1/3}MnO_3/BiFeO_3$ Heterostructure. *Appl. Phys. Lett.* **2014**, *105*, 112406.
(20) Yu, P.; Lee, J. S.; Okamoto, S.; Rossell, M. D.; Huijben, M.; Yang, C. H.; He, Q.; Zhang, J. X.; Yang, S. Y.; Lee, M. J.; Ramasse, Q. M.; Erni, R.; Chu, Y. H.; Arena, D. A.; Kao, C. C.; Martin, L. W.; Ramesh, R. Interface Ferromagnetism and Orbital Reconstruction in $BiFeO_3$-$La_{0.7}Sr_{0.3}MnO_3$ Heterostructures. *Phys. Rev. Lett.* **2010**, *105*, 027201.
(21) Borisevich, A. Y.; Chang, H. J.; Huijben, M.; Oxley, M. P.; Okamoto, S.; Niranjan, M. K.; Burton, J. D.; Tsymbal, E. Y.; Chu, Y. H.; Yu, P.; Ramesh, R.; Kalinin, S. V.; Pennycook, S. J. Suppression of Octahedral Tilts and Associated Changes in Electronic Properties at Epitaxial Oxide Heterostructure Interfaces. *Phys. Rev. Lett.* **2010**, *105*, 087204.
(22) Neumann, R. F.; Bahiana, M.; Binggeli, N. Magnetic Properties of $La_{0.67}Sr_{0.33}MnO_3/BiFeO_3(001)$ Heterojunctions: Chemically Abrupt vs. Atomic Intermixed Interface. *EPL* **2012**, *100*, 67002.
(23) Hatt, A. J.; Spaldin, N. A.; Ederer, C. Strain-Induced Isosymmetric Phase Transition in $BiFeO_3$. *Phys. Rev. B* **2010**, *81*, 054109.
(24) Chu, Y. H.; Martin, L. W.; Holcomb, M. B.; Ramesh, R. Controlling Magnetism with Multiferroics. *Mater. Today* **2007**, *10*, 16−23.
(25) Zhang, J. X.; He, Q.; Trassin, M.; Luo, W.; Yi, D.; Rossell, M. D.; Yu, P.; You, L.; Wang, C. H.; Kuo, C. Y.; Heron, J. T.; Hu, Z.; Zeches, R. J.; Lin, H. J.; Tanaka, A.; Chen, C. T.; Tjeng, L. H.; Chu, Y. H.; Ramesh, R. Microscopic Origin of the Giant Ferroelectric Polarization in Tetragonal-Like $BiFeO_3$. *Phys. Rev. Lett.* **2011**, *107*, 147602.
(26) Sun, M. Y.; Li, P.; Jin, C.; Wang, L. Y.; Zheng, D. X.; Bai, H. L. Enhanced Exchange Bias in Fully Epitaxial Fe_3O_4/Tetragonal-Like $BiFeO_3$ Magnetoelectric Bilayers. *EPL* **2014**, *105*, 17007.
(27) Kohn, W.; Sham, L. J. Self-Consistent Equations Including Exchange and Correlation Effects. *Phys. Rev.* **1965**, *140*, A1133−A1138.
(28) Blöchl, P. E. Projector Augmented-Wave Method. *Phys. Rev. B* **1994**, *50*, 17953−17979.
(29) Kresse, G.; Furthmüller, J. Efficient Iterative Schemes for Ab Initio Total-Energy Calculations Using a Plane-Wave Basis Set. *Phys. Rev. B* **1996**, *54*, 11169−11186.
(30) Perdew, J. P.; Burke, K.; Ernzerhof, M. Generalized Gradient Approximation Made Simple. *Phys. Rev. Lett.* **1996**, *77*, 3865−3868.
(31) Wang, C.; Stojić, N.; Binggeli, N. Optimal Interface Doping at $La_{2/3}Sr_{1/3}MnO_3/SrTiO_3(001)$ Heterojunctions for Spintronic Applications. *Appl. Phys. Lett.* **2013**, *102*, 152414.
(32) Ferrari, V.; Pruneda, J. M.; Artacho, E. Density functional and half-metallicity in $La_{2/3}Sr_{1/3}MnO_3$. *Phys. Status Solidi (a)* **2006**, *203*, 1437−1441.
(33) Tütüncü, H. M.; Srivastava, G. P. Electronic Structure and Lattice Dynamical Properties of Different Tetragonal Phases of $BiFeO_3$. *Phys. Rev. B* **2008**, *78*, 235209.
(34) Singh, M. K.; Ryu, S.; Jang, H. M. Polarized Raman Scattering of Multiferroic $BiFeO_3$ Thin Films with Pseudo-Tetragonal Symmetry. *Phys. Rev. B* **2005**, *72*, 132101.
(35) Sando, D.; Barthélémy, A.; Bibes, M. $BiFeO_3$ Epitaxial Thin Films and Devices: Past, Present and Future. *J. Phys.: Condens. Matter* **2014**, *26*, 473201.
(36) Wang, D. H.; Goh, W. C.; Ning, M.; Ong, C. K. Effect of Ba Doping on Magnetic, Ferroelectric, and Magnetoelectric Properties in Multiferroic $BiFeO_3$ at Room Temperature. *Appl. Phys. Lett.* **2006**, *88*, 212907.
(37) Tsui, F.; Smoak, M. C.; Nath, T. K.; Eom, C. B. Strain-Dependent Magnetic Phase Diagram of Epitaxial $La_{0.67}Sr_{0.33}MnO_3$ Thin Films. *Appl. Phys. Lett.* **2000**, *76*, 2421.
(38) Autieri, C.; Sanyal, B. Unusual Ferromagnetic $YMnO_3$ Phase in $YMnO_3/La_{2/3}Sr_{1/3}MnO_3$ Heterostructures. *New J. Phys.* **2014**, *16*, 113031.
(39) Ranke, W.; Ritter, M.; Weiss, W. Crystal Structures and Growth Mechanism for Ultrathin Films of Ionic Compound Materials: FeO(111) on Pt(111). *Phys. Rev. B* **1999**, *60*, 1527−1530.
(40) Palai, R.; Katiyar, R. S.; Schmid, H.; Tissot, P.; Clark, S. J.; Robertson, J.; Redfern, S. A. T.; Catalan, G.; Scott, J. F. β Phase and γ-β Metal-Insulator Transition in Multiferroic $BiFeO_3$. *Phys. Rev. B* **2008**, *77*, 014110.
(41) Perdew, J. P.; Parr, R. G.; Levy, M.; Balduz, J. L., Jr Density-Functional Theory for Fractional Particle Number: Derivative Discontinuities of the Energy. *Phys. Rev. Lett.* **1982**, *49*, 1691−1694.
(42) Maurice, J. L.; Pailloux, F.; Barthélémy, A.; Durand, O.; Imhoff, D.; Lyonnet, R.; Rocher, A.; Contour, J. P. Strain Relaxation in the Epitaxy of $La_{2/3}Sr_{1/3}MnO_3$ Growth by Pulsed-Laser Deposition on $SrTiO_3(001)$. *Philos. Mag.* **2003**, *83*, 3201−3224.
(43) Kuo, H. H.; Chen, L.; Ji, Y. Z.; Liu, H. J.; Chen, L. Q.; Chu, Y. H. Tuning Phase Stability of Complex Oxide Nanocrystals via Conjugation. *Nano Lett.* **2014**, *14*, 3314−3320.

DOI: 10.1021/acsami.5b02436
ACS Appl. Mater. Interfaces 2015, 7, 10612−10616